Evolution of Microstructure during Fabrication of Zr-2.5 Wt pct Nb Alloy Pressure Tubes

D. SRIVASTAVA, G.K. DEY, and S. BANERJEE

Microstructural changes occurring during the fabrication of Zr-2.5 pct Nb alloy pressure tubes by a modified route, involving hot extrusion followed by two pilgering operations with an intermediate annealing step, have been examined in detail. In the conventional fabrication route, the hot extrusion step is followed by a single cold drawing operation in which the cold work to the extent of 25 pct is imparted to the material for achieving the required mechanical properties. Tensile properties obtained at each stage of fabrication have been evaluated and compared between the two processes. The main aim of this work has been to produce a microstructure and texture which are known to yield a lower irradiation growth. Additionally, suitable annealing conditions have been optimized for the intermediate annealing which annihilates the cold work introduced by the first cold pilgering operation without disturbing the two-phase elongated microstructure. This elongated $\alpha + \beta_I$ microstructure is required for obtaining the desired level of strength at 310 °C. The final microstructure and the crystallographic texture of the finished pressure tube have been compared with those reported for the conventionally processed material.

I. INTRODUCTION

Zr-2.5 pct Nb alloy is presently being used as a pressure tube material in pressurized heavy water reactors. The satisfactory performance and the life of the pressure tube depend mainly upon its dimensional stability in the reactor, which is a strong function of several metallurgical parameters. These parameters include the shape, the size and the size distribution of the grains, the distribution of various phases, the interfacial structure, and the crystallographic texture.[1–10] The fabrication of pressure tubes involves a large number of thermomechanical treatments, and the final microstructure developed as a result of these fabrication steps determines the long-term and short-term properties of these tubes. It is important to understand the influence of each of these fabrication steps on microstructure and crystallographic texture in order to optimize the pressure tube fabrication flow sheet. The conventional method of fabrication of these tubes involves hot extrusion followed by 25 pct cold drawing (Figure 1).[1] There has been continuous effort toward improving the resistance to irradiation induced growth through the modification of the microstructure of the pressure tube material.[2] Fleck *et al.*[2] have studied the change in microstructure and its effect on the properties by altering the conventional route. In the present work, a modified route has been examined for the production of pressure tubes, which involves hot extrusion of lower extrusion ratio and two-stage pilgering with an intermediate annealing treatment (Figure 1). This modified route offers the following advantages.

(a) A lower extrusion ratio results in a lower aspect ratio of the α grains, causing an improvement in the resistance to irradiation growth.[6] This also results in the less intense circumferential basal pole texture.
(b) The two-stage cold pilgering process ensures a better control of the dimensional tolerances of the finished tubes.
(c) During the hot extrusion, the microstructure and the mechanical properties of the leading end to the trailing end vary due to the variation in the hot working temperature.

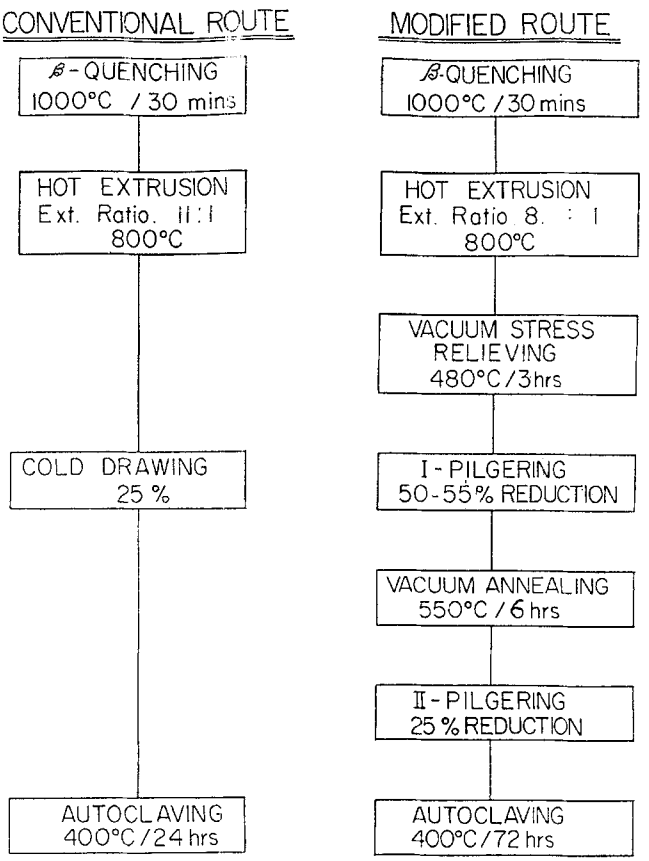

Fig. 1—The conventional and modified fabrication flow sheets of Zr-2.5 pct Nb alloy pressure tubes.

D. SRIVASTAVA, Scientific Officer, G.K. Dey, Scientific Officer, and S. BANERJEE, Head, are with the Metallurgy Division, Bhabha Atomic Research Center BARC, Bombay 400 085, India. G.K. DEY is presently on leave from BARC, is Postdoctoral Fellow, Department of Materials Science and Engineering, University of Cincinnati, Cincinnati, OH-45221.
Manuscript submitted September 18, 1992.

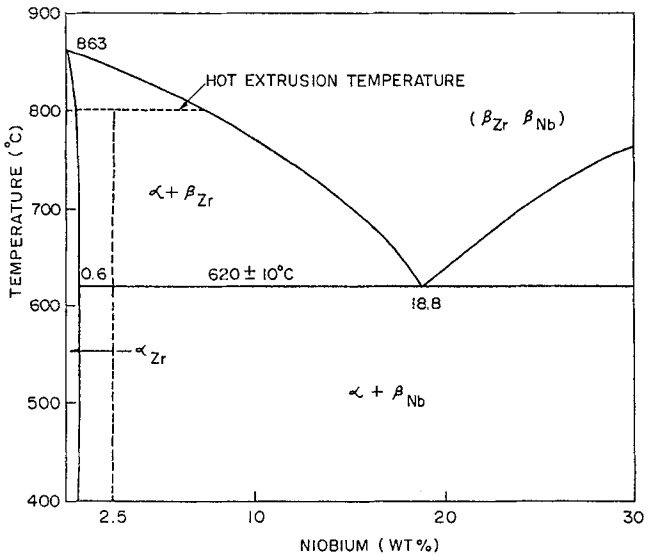

Fig. 2—The phase diagram of the binary Zr-Nb binary system.[9]

Table I. Chemical Composition of the Zr-2.5 pct Nb Alloy

Niobium (Wt Pct)	Oxygen (ppm)	Iron (ppm)	Hydrogen (ppm)	Nitrogen (ppm)
2.51	1092	1250	<10	30

Additional cold working and annealing treatment levels off this variation considerably.

(d) Batch to batch variation in composition and the hot working process variables within the limits of specification cause the variation in mechanical properties of as-extruded tubes. Modified route provides a finer control on the microstructure and the mechanical properties through a proper selection of the annealing temperature.

(e) Due to the reasons mentioned earlier, the scatterband of the mechanical properties of the finished tubes has been found to be narrower for the modified fabrication route. This has resulted in higher material yields in production.

The main aim of this work has been to examine whether tubes produced by the modified route can qualify in terms of microstructure, dislocation density, crystallographic texture, and short-term mechanical properties at 310 °C as specified for the conventionally processed material.

In the present work, the evolution of microstructure during each fabrication step of the modified route has been studied by optical microscopy, scanning electron microscopy (SEM), and transmission electron microscopy (TEM) on both longitudinal and transverse sections of pressure tubes. In addition, the tensile properties have been determined at each stage of fabrication and compared with those reported for the conventionally processed material. The equilibrium structure of the Zr-2.5 pct Nb alloy consists of a two-phase (α + β_{II}) mixture (Figure 2).[11] The thermodynamics of equilibrium and metastable phase reactions in the Zr-Nb system have been studied by Menon *et al.*[12] It has been shown that the phase separation tendency of the β phase (into Zr-rich (β_I) and Nb-rich (β_{II}) constituents) influences the microstructure evolution over the entire composition range in this system. The distribution of the α and β phases in the hot-extruded microstructure and the nature of the interfaces between the two phases have recently been investigated in detail.[8,9,13–15]

The literature on dynamic and static recrystallization of a two-phase microstructure is rather limited. Since both the recrystallization processes are important in context of the modified route, the occurrence of the former during the hot extrusion step and that of the latter during the annealing step have been investigated in the present study.

It is recognized that the metastable β_I phase present in the hot-extruded material, which is enriched with niobium up to a level of 15 to 20 pct, does not decompose into the equilibrium products, *i.e.*, α and Nb-rich β_{II} phase, due to a large free energy barrier associated with the enrichment of the β_I phase with niobium.[12] It is due to this reason that the β_I stringers in the hot-extruded Zr-2.5 pct Nb alloy remain essentially untransformed during the course of annealing treatments at temperatures below the monotectoid temperature.[1] Precipitation of the ω phase could be expected to occur in β_I phase of such composition during subsequent annealing. The possible occurrence of ω precipitation within the β_I phase has been investigated in the present work.

II. EXPERIMENTAL PROCEDURE

Samples of the Zr-2.5 pct Nb alloy were obtained from different stages of fabrication of pressure tubes. The chemical composition of the alloy is given in Table I. Samples were cut in both longitudinal and transverse directions for examination of microstructures. Samples for light microscopy were chemically etched in a 5 pct HF + 45 pct HNO_3 solution and those for SEM in a 8 pct HF + 45 pct HNO_3 solution. Disc samples of 3-mm diameter for TEM examination were punched out from mechanically thinned specimens and jet electrothinned at 20 V in a solution containing 30 parts perchloric acid, 170 parts *n*-butyl alcohol, and 300 parts methanol, maintained at −35 °C. The examination was carried out in a JEOL* 2000FX microscope. The chemical analysis of the α and β phases was carried out by energy dispersive spectroscopy (EDS) in a Philips** 430T microscope. The volume fractions of the two phases as well as the thicknesses and the aspect ratios of these two phases were estimated using a digital image processor. Samples for crystallographic texture evaluation were cut in three principal directions, axial, radial, and circumferential, from the pressure tube. An adequate number of these strips were mounted together to provide sufficient surface area for X-ray diffraction. The layers representing the three principal directions were polished mechanically as well as chemically for the X-ray diffraction experiments.

*JEOL is a trademark of Japan Electron Optics Ltd., Tokyo.

**PHILIPS is a trademark of Philips Electron Instruments.

III. RESULTS AND DISCUSSION

β-Quenched Structure

The arc-melted Zr-2.5 pct Nb cast ingot is initially hot forged or hot extruded and the worked billet is soaked at

1000 °C for 30 minutes in the β-phase field. The soaked ingot is quenched in water which ensures chemical homogenization, randomization of the texture, and refinement of the grain size.

The microstructure produced after quenching consisted of acicular martensite with coarse primary plates (Figure 3(a)) and later generation plates having continuously decreasing dimensions (Figure 3(b)). Such a morphology results from a continuous partitioning of the β phase by martensite plates and the autocatalytic nucleation of the next generation of plates. Contrary to earlier reports pertaining to alloys of similar compositions,[16,17] it was observed that most of the primary plates were not internally twinned. This is not unexpected since the cooling rate achieved in the β-quenching operation of 12-mm-thick extruded tubes would be much lower than those used in most of the earlier studies.[15,16,17] In order to examine the influence of the quenching rate on the morphology of the martensite in this alloy, a 2-mm-thick slice was β quenched. This sample showed the internally twinned martensite plates (Figures 4(a) through (c)) clearly demonstrating the influence of the cooling rate. The arrangement of the primary martensite plates and the stacking of later generation plates in the partitioned volume were governed by self-accommodation of shape strains associated with a group of martensite plates.[18] The finest martensite units, which formed toward the end of the transformation, were laths stacked in a parallel array within colonies, the alternate laths in a colony being twin related (Figure 4(d)). Analysis, and dark-field imaging failed to show the presence of any retained β phase in the β-quenched Zr-2.5 pct Nb pressure tube alloy. It has been shown in a previous work[9] that a Widmanstätten structure is produced in this material after β quenching. It is possible that the quenching rates used in this investigation were much lower than that used in the present work. A through-thickness examination of the microstructure of the samples obtained from β-quenched tubes showed that the martensite structure was present across the entire cross section.

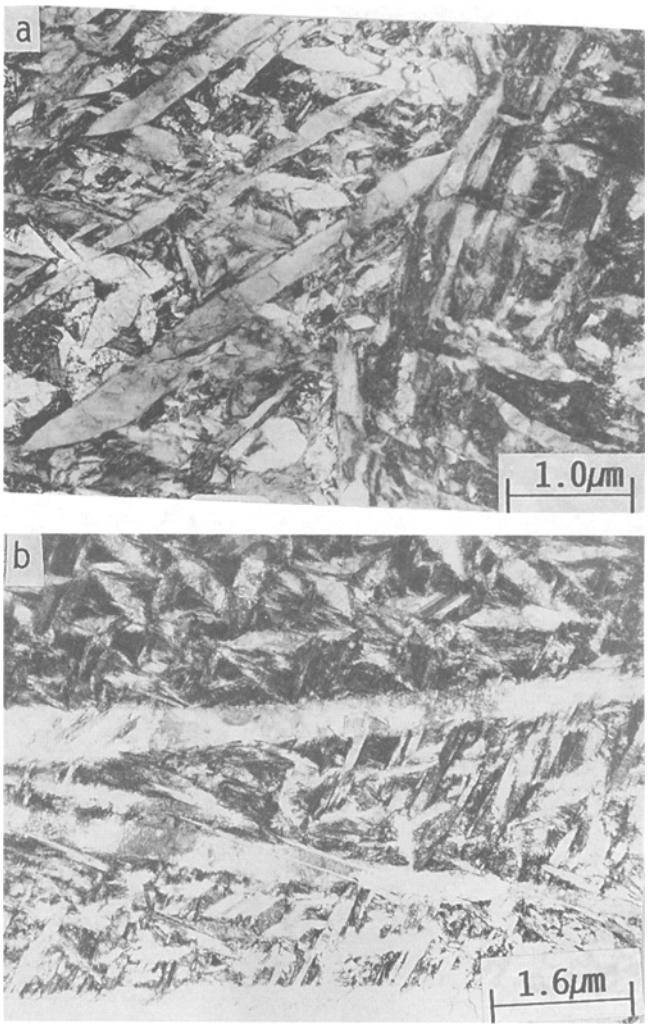

Fig. 3—(*a*) A representative view of the acicular martensite plates in the β-quenched alloy. (*b*) Distribution of the large primary and the fine secondary martensite plates in the β-quenched alloy.

IV. HOT-EXTRUDED STRUCTURE

Hot extrusion is carried out in the $\alpha + \beta_I$ phase field and the hot extrusion temperature controls the composition and the volume fraction of the α and β_I phases. Figure 5 shows typical optical and SEM microstructure of the hot-extruded tube in the longitudinal and transverse sections. An extrusion ratio of 8:1 and an extrusion temperature of 800 °C are employed for processing this tube. The longitudinal section shows the β_I-phase stringers elongated in the extrusion direction (dark etching in light microscopy and bright in secondary electron images in the SEM). The morphology and distribution of the two phases α and β_I are similar to those reported for extruded tubes processed by conventional fabrication route.[1–5] The grain structure of the α and β_I phases is not revealed in these micrographs. Quantitative analyses of volume fraction, aspect ratio, and grain size of the α and β_I phases obtained in the extruded microstructure of the modified route are presented and compared with those of conventionally processed material in Table II. The lower values of the aspect ratio of the α-phase and β_I-phase stringers are due to a lower extrusion ratio in the modified route. It has been observed and estimated by Holt and Ibrahim[7] that irradiation growth would be more in the direction along which α grains are elongated and an equiaxed structure would be an ideal grain shape for minimizing the irradiation growth. Therefore, α grain with lower aspect ratio would help in reducing the irradiation growth in the axial direction.

Comparing the measured volume fraction of the β_I phase in the hot-extruded tubes and that estimated from the phase diagram at 800 °C, it could be seen that the β_I volume fraction decreased from 35 pct to about 20 to 28 pct during cooling from the extrusion temperature (Table II). The observed volume fraction of the β_I phase (20 to 28 pct) in the Zr-2.5 pct Nb alloy corresponds to a niobium concentration of 8 to 12 pct in this phase (Table II), and this was confirmed by EDS. Therefore, β phase present in the hot-extruded and subsequent-annealed structure is essentially a metastable β_I phase instead of the equilibrium β_{II} phase. In the conventionally processed hot-extruded material, a higher niobium content (18 to 20 pct) in the β_I phase (corresponding to a β_I volume fraction of 11 to 13 pct) is reported. This difference can be attributed to a higher cooling rate experienced during cooling after the hot extrusion pro-

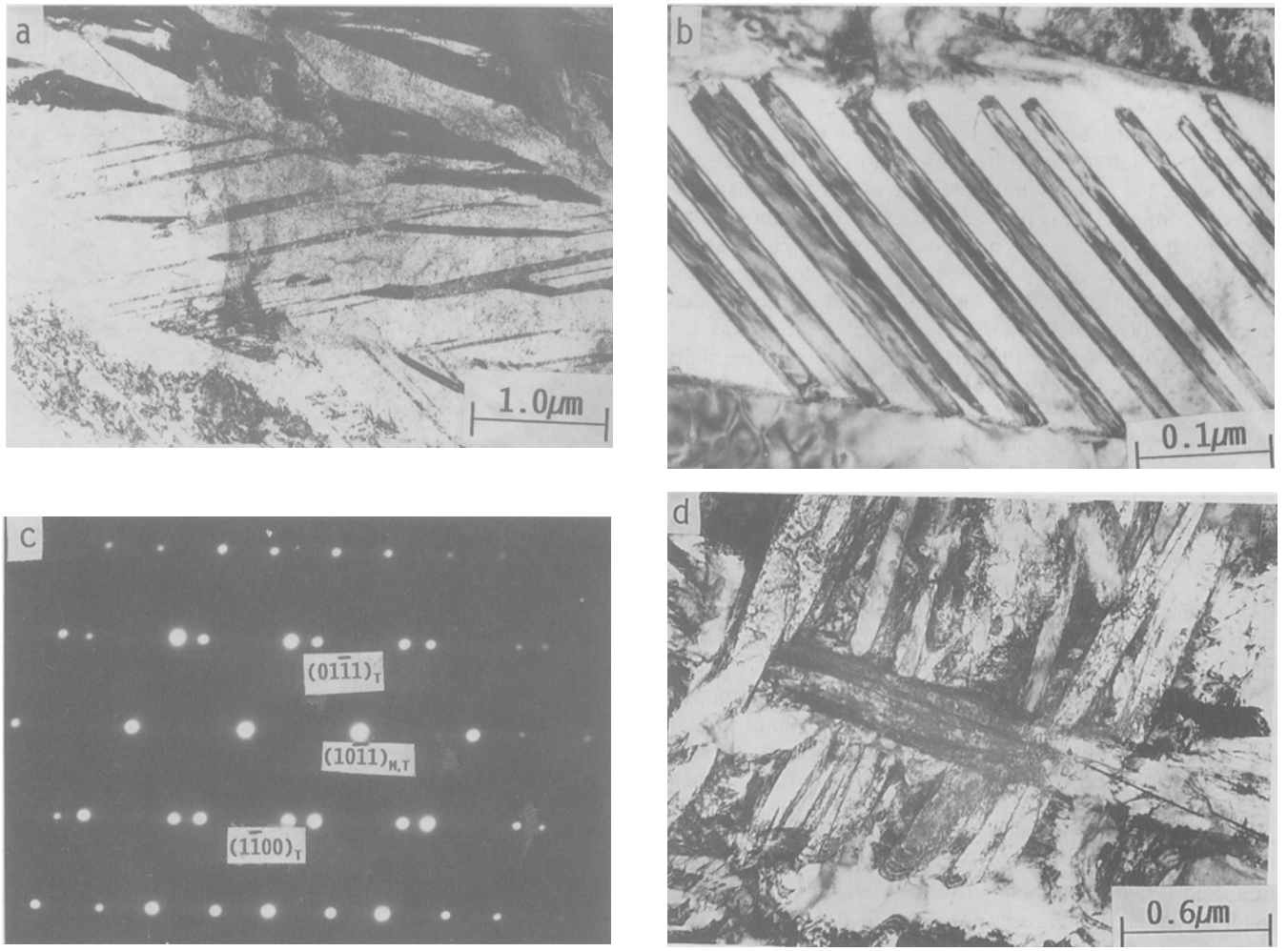

Fig. 4—(*a*) Micrograph showing the presence of a relatively large fraction of internally twinned primary plates obtained at higher cooling rates. (*b*) Internally twinned martensite plates showing stacks of $\{10\bar{1}1\}_{\alpha'}$ twins. (*c*) SAD pattern obtained from the internally twinned regions showing $\{1011\}_{\alpha'}$ twinning plane. (*d*) Packets of near parallel stacked lath martensite.

cess in the modified route. In the modified route, the hot-extruded tubes are cooled by water spraying unlike the air cooling adopted in the conventional route. This rapid cooling restricts the partitioning of niobium between the α and β_I phases. A higher volume fraction of the β_I phase corresponds to a larger fraction of the α/β_I interfaces in the microstructure of the tubes processed by a modified route. Such a microstructure is expected to be more favorable from the consideration of the strength as well as creep properties.

Typical TEM micrographs of the hot-extruded structure in the longitudinal and transverse sections are shown in Figures 6(a) and (b), respectively. It is clear from these micrographs that the α stringers were essentially made up of a series of equiaxed α grains. This observation strongly suggested the operation of a dynamic recrystallization process within the α phase during hot extrusion. The grain structure of the β_I phase could not be revealed in bright-field microscopy. However, with the help of dark-field microscopy (Figures 6(c) and (d)), it was possible to image individual β_I grains with sharp high-angle boundaries, suggesting that the β_I phase too experienced dynamic recrystallization during hot extrusion. This is in agreement with Chakravorthy *et al.*,[19] who showed dynamic recrystallization in this alloy at 750 °C and at a strain rate of 0.001. The fact that dynamic recrystallization was not complete in all regions could be inferred from the micrograph in Figures 7(a) and (b), which shows the occurrence of a dynamically recovered, polygonized structure within an α-phase stringer. However, the volume fraction of such unrecrystallized regions was found to be much smaller than the recrystallized regions.

The SAD patterns obtained from β_I grains often showed the presence of ω-phase reflections. The characteristic mottled appearance of the β_I grains also suggested the presence of the ω phase. The dark-field micrograph (Figure 8(a)) obtained with $\{1\bar{1}00\}_\omega$ reflections shows the presence of fine precipitates of the phase within the β_I grain. The SAD patterns with $\langle 113\rangle_{\beta I}$ and $\langle 110\rangle_{\beta I}$ zone axes are shown in Figures 8(b) and (c), respectively. These patterns exhibit distinct ω reflections along with β_I reflections. Since the β_I phase in the hot-extruded Zr-2.5 pct Nb alloy contained 8 to 10 pct Nb, the occurrence of the ω phase in the β_I regions was not unexpected, as in this composition range, both the athermal and the aged ω phase are known to form.[20,21] The intensity of the ω reflections varied considerably from one grain to another, implying that niobium content in different β_I grains was not always the same. It is interesting to note

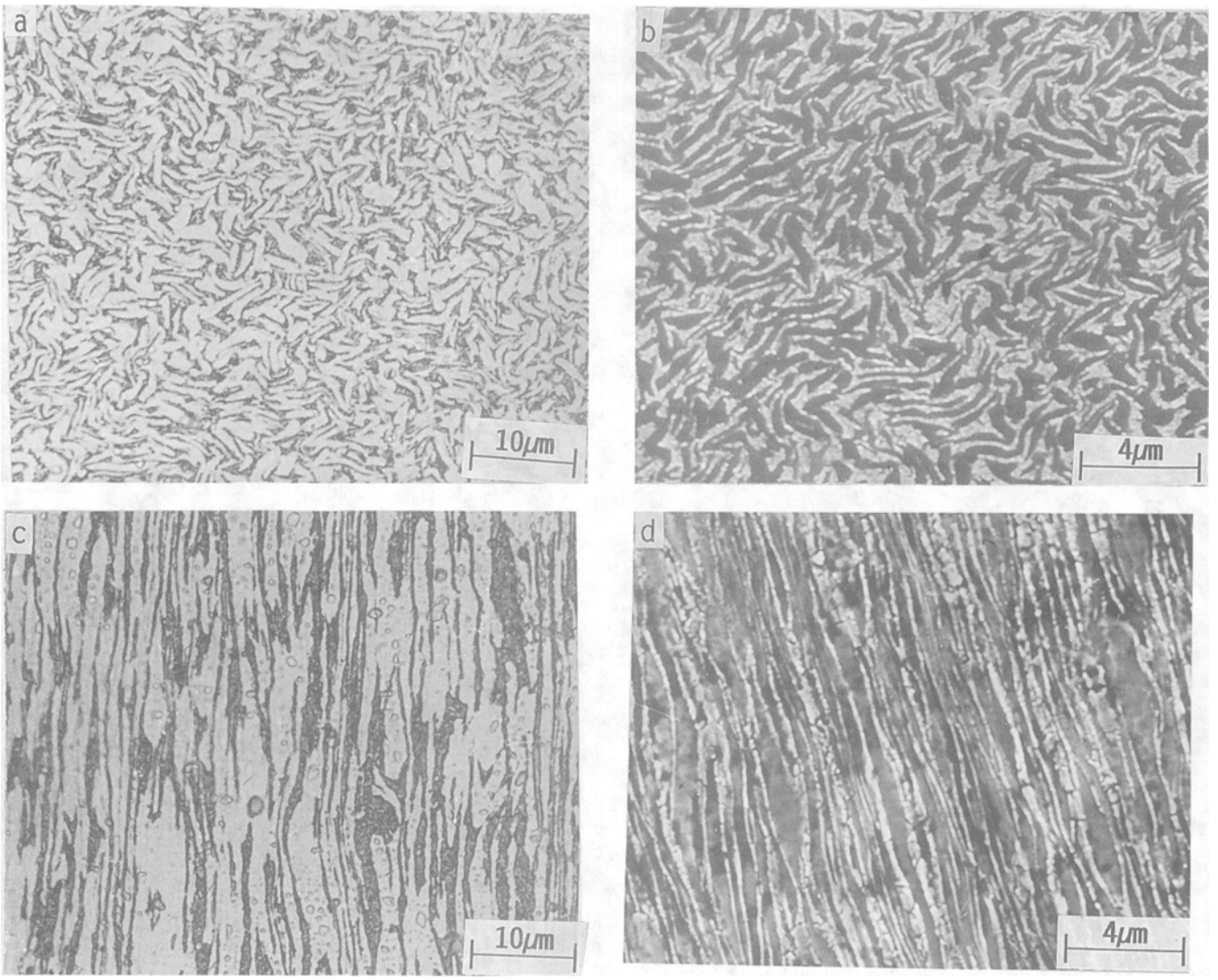

Fig. 5—Optical and SEM micrographs of the two-phase ($\alpha + \beta_I$) microstructure, showing (*a*) and (*b*) elongated morphology in the longitudinal section and (*c*) and (*d*) sereted morphology in the transverse section of a hot-extruded tube. Note: α phase is bright in optical and dark in SEM.

Table II. Microstructural Parameters of the Hot-Extruded Structure

Microstructural Parameters		Modified Route		Conventional Route[1]
		α phase	β phase	α phase
Grain size	length (μm)	10 to 15	5 to 8	20
	width (μm)	0.8 to 1.4	0.1 to 0.2	2
	Aspect ratio	6 to 10	50 to 80	10
	thickness (μm)	0.2 to 0.4	<0.02	0.04
Volume fraction (pct)	estimated at 800 °C	65	35	—
	experimentally measured	72 to 80	20 to 28	87 to 89*
	from phase diagram	0.2	7.0	
Niobium content (pct)	from measured volume fraction	0.2	8 to 12	18 to 20
	estimated by EDS	<1.0	10.0	

*Estimated on the basis of β-phase composition.

that in some of the SAD patterns, additional reflections were present in both $\langle 113 \rangle_{\beta I}$ and $\langle 110 \rangle_{\beta I}$ zones similar to those reported for the ordered ω phase observed by Strychor and Williams[22] and Benderskey *et al.*[23] in Ti-Al-Nb alloy system. This observation was not consistent with that reported in the literature on ω-phase formation in Zr-Nb alloys.[20,21] The occurrence of an ordered phase was not expected in Zr-2.5Nb alloy since the ordering of the bcc (β_I) phase is not reported. The present observation suggested a B2 (CsCl) type ordering in the β_I phase which,

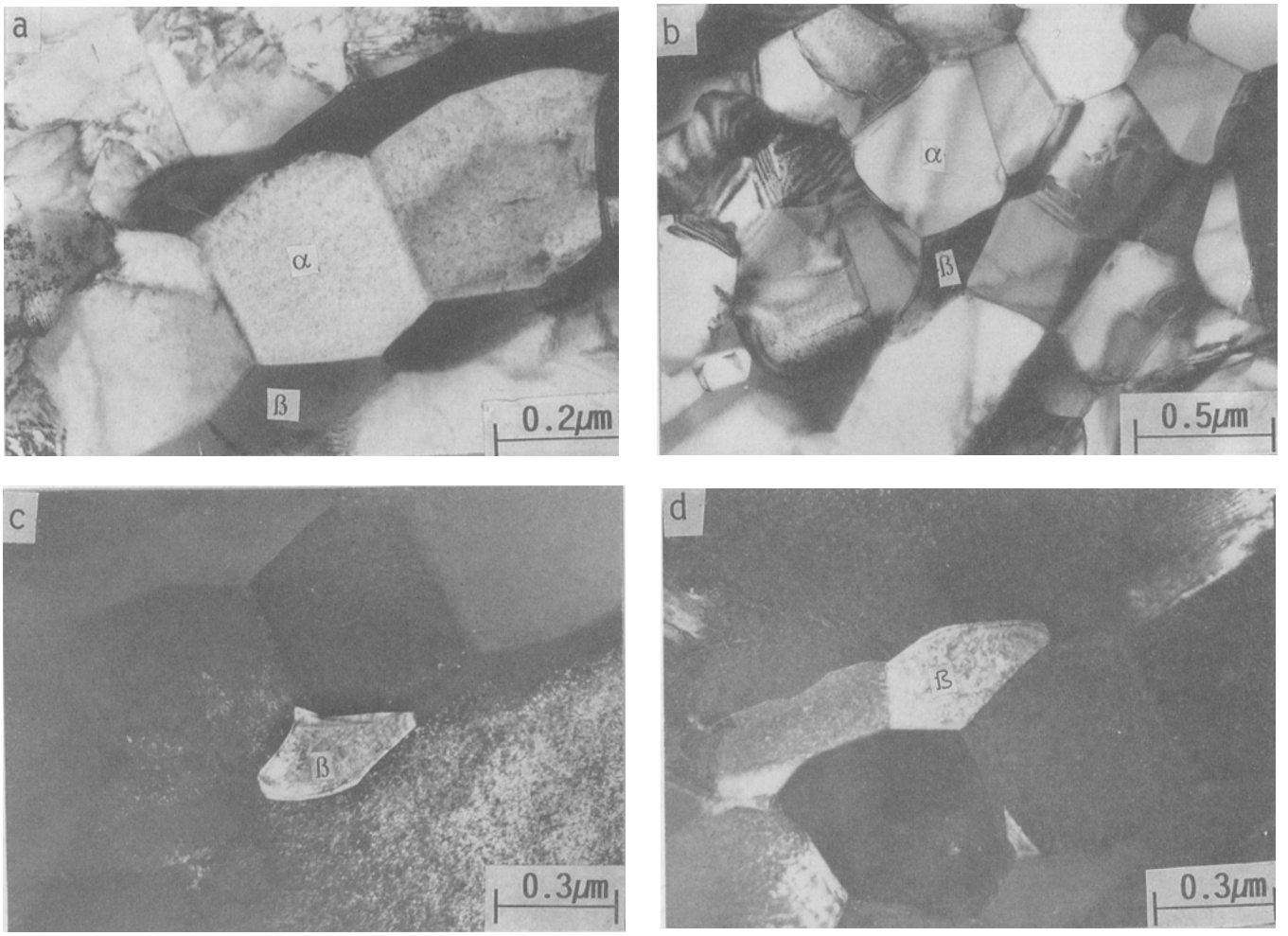

Fig. 6—(*a*) and (*b*) TEM micrographs showing dynamically recrystallized equiaxed α grains within α stringers. The β_I phase is present between the α stringers in the (a) longitudinal and (b) transverse sections. (*c*) Dark-field micrograph obtained from $\{110\}_{\beta I}$ reflection showing dynamically recrystallized β phase. (*d*) Dark-field micrograph showing wetting of the α/α grain boundaries by the β_I phase.

in turn, caused a chemical ordering of the ω phase. It is likely that the presence of impurity like iron was responsible for inducing the chemical order in the ω phase.

The tensile properties of the extruded tubes following both the modified and conventional routes[1,2,3] are presented in Tables III(a) and (b), respectively. It can be seen that the tensile properties in both cases are very similar, even though the grain morphologies are slightly different due to two different extrusion ratios.

V. FIRST PILGERED STRUCTURE

During this stage of pressure tube fabrication, 50 to 55 pct cold work is introduced by a pilgering operation in which a large reduction in wall thickness is achieved with little reduction in the tube diameter. This kind of fabrication practice is known to alter the crystallographic texture of zirconium alloys quite substantially.[9,23-24] In a pilgering operation, the basal plane poles tend to become aligned along the direction of compressive stress. A detailed account of the changes in the crystallographic texture at different stages of the modified fabrication route has been provided by Haq *et al.*[25] No pronounced change in crystallographic texture was noticed in samples obtained from pressure tubes subjected to the first pilgering step. This is possibly due to the fact that the two-phase $\alpha + \beta_I$ elongated microstructure was not amenable for the grain rotation necessary for bringing about a significant change in texture.

The morphologies of individual α and β_I stringers after the first pilgering step were difficult to resolve under light microscopy or SEM, as these stringers were further elongated in the direction of working. However, the aspect ratio of the α grain was increased marginally. Fragmentation of the stringers also occurred due to the heavy cold deformation. Transmission electron microscopy observations revealed a very high dislocation density within the α stringers which were separated by very thin β_I stringers. The α/β_I interfaces were quite sharp. These features were observed in samples corresponding to both longitudinal and transverse sections of the tube (Figures 9(a) and (b)). The distribution of dislocations was found to be nonuniform, with a great majority of them being concentrated close to the α/β_I interfaces.

The tensile properties of the first pilgered tube are presented in Table III(a). Considerable increase in yield strength and ultimate tensile strength and a corresponding decrease in elongation value had occurred due to the cold work introduced during the pilgering operation.

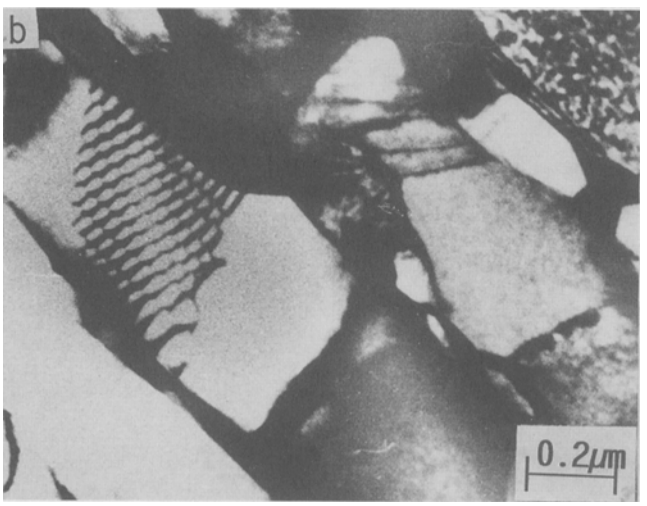

Fig. 7—(*a*) Dynamically recovered α stringers. (*b*) Low energy configuration of dislocation arrays in the dynamically recovered α stringers.

VI. MICROSTRUCTURE AFTER INTERMEDIATE ANNEALING

The optimum combination of tensile strength and in-reactor creep behavior is achieved in Zr-2.5 pct Nb pressure tubes by introducing 20 to 25 pct cold work[26,27] in the final stage of fabrication to produce a dislocation density of about 2.5×10^{14} /m^2. The purpose of the intermediate annealing treatment prior to the second pilgering is to annihilate all the cold work introduced in the first pilgering step. The annealing temperature was varied between 500 °C to 650 °C and annealing duration varied between 1 to 6 hours. It was observed that the elongated two-phase structure could be retained only if the annealing temperature was kept below 575 °C. Retention of this structure was necessary for obtaining optimum tensile properties at the service temperature of 310 °C.

Microstructural changes that occurred during the annealing process could be seen from Figure 10, which shows the

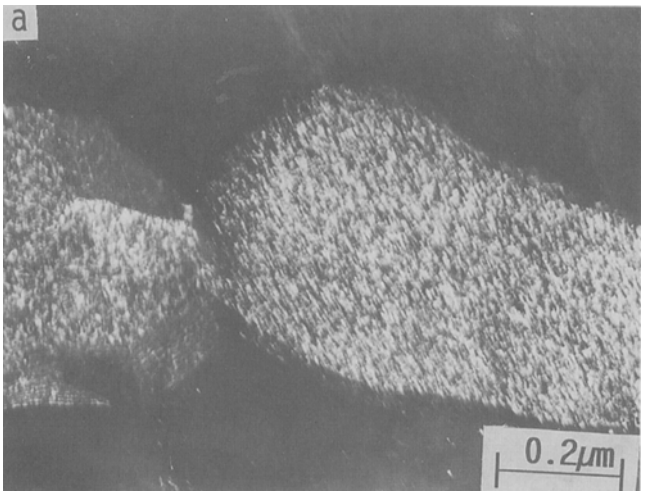

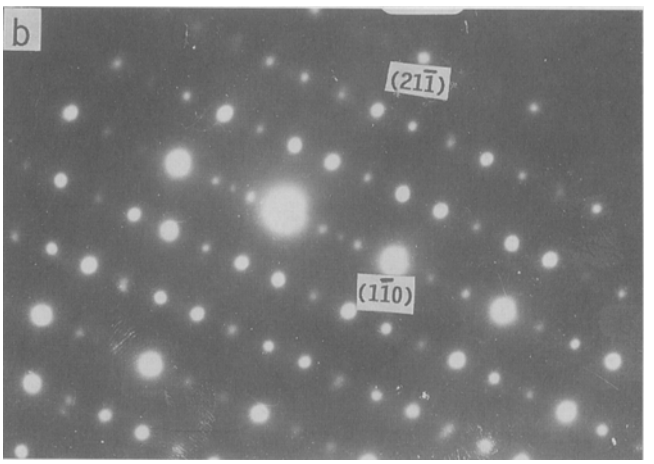

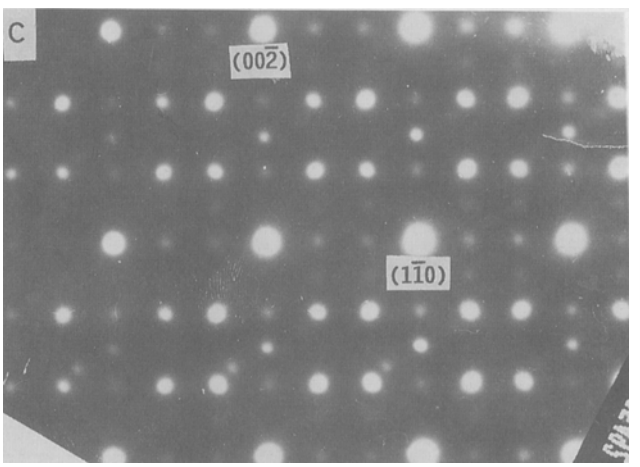

Fig. 8—(*a*) Dark-field micrograph showing distribution of fine ω particles within the β_I phase (obtained with a $\{1\bar{1}00\}_\omega$ reflection). (*b*) and (*c*) SAD patterns corresponding to $\langle 113\rangle_{\beta I}$ and $\langle 110\rangle_{\beta I}$ zone axes, respectively, showing the presence of extra reflections of the ordered ω phase.

annealed microstructure developed at 500 °C, 550 °C, and 600 °C. Annealing at 500 °C even for 6 hours did not recrystallize the α stringers, as could be seen from the presence of a high dislocation density within them (Figure 10(a)). Recovery of the α stringers resulted in the formation of the subgrains and low energy configuration of the dislocation arrays. It can be seen from Table IV that the an-

Table III. Mechanical Properties at 310 °C after Different Stages of Fabrication

Fabrication Stage	UTS (MPa)	YS(0.2 pct) (MPa)	Total Elongation
(a) Modified Route			
Hot extruded	449	360	20
First pilgered	556	390	17
Annealed 550 °C	437	337	18
Second pilgered and autoclaved	520	386	18
(b) Conventional Route[2]			
Fabrication Stage	UTS (MPa)	YS(0.2 pct) (MPa)	Total Elongation
Hot extruded	434	365	22
Cold drawn (20 pct)	482	427	12
Stress relieved 400 °C/24 h	468	344	14

Note: UTS = ultimate tensile strength and YS = yield strength.

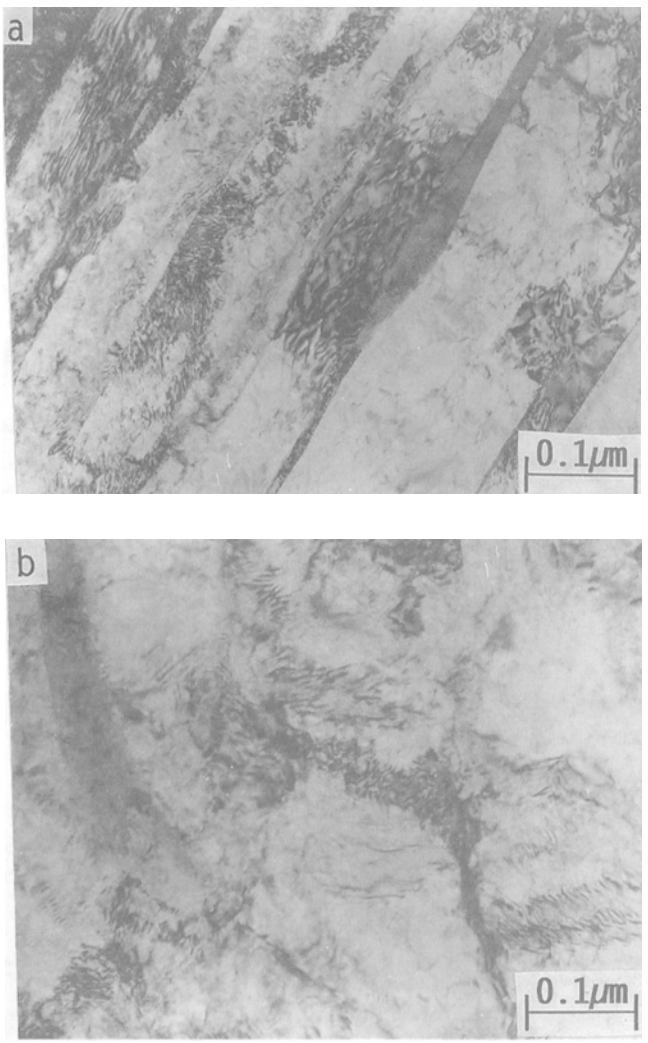

Fig. 9—First pilgered microstructure illustrating the very high dislocation density. The dislocations are concentrated mainly to the α/β_i interface in (*a*) longitudinal and (*b*) transverse sections, respectively.

nealing treatment at 500 °C for 6 hours has not brought down the tensile strength to the level of the hot-extruded material and the elongation value was also substantially

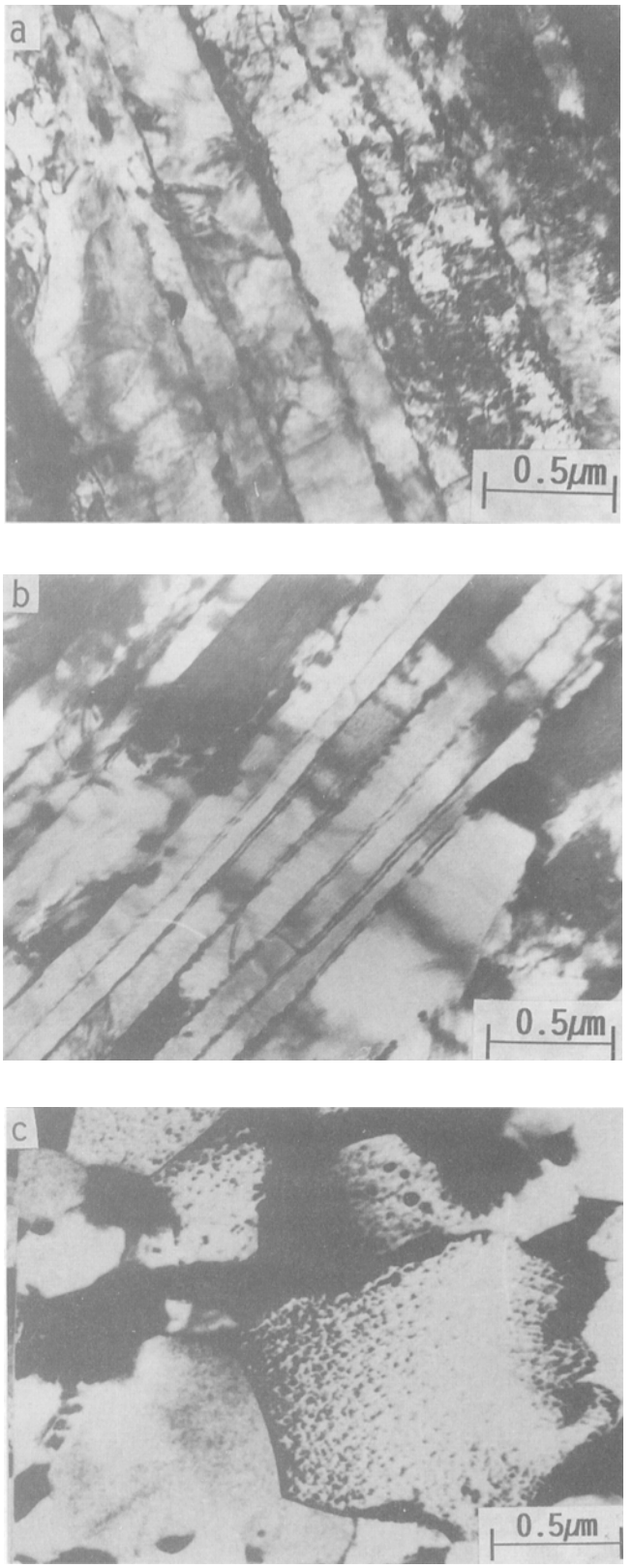

Fig. 10—(*a*) Incomplete recrystallization of the α stringers, as evidenced by the presence of a substantial number of dislocations after annealing at 500 °C for 6 h. (*b*) Completely recrystallized microstructure obtained after annealing at 550 °C for 3 h. The lamellar morphology of the two phases is not affected by this annealing treatment. (*c*) Micrograph showing the coarsening of the α grains and the redistribution of the β_i phase predominantly at the trijunctions of the α grains after annealing at 600 °C for 1 h.

Table IV. Mechanical Properties at Room Temperature as a Function of Annealing Parameters[32]

Annealing Parameters	UTS (MPa)	YS(0.2 pct) (MPa)	Total Elongation
As extruded	657	492	27
Cold worked (55 pct)	875	607	17
500 °C 6 h	722	569	22
550 °C 6 h	598	455	17
600 °C 0.5 h	630	527	14

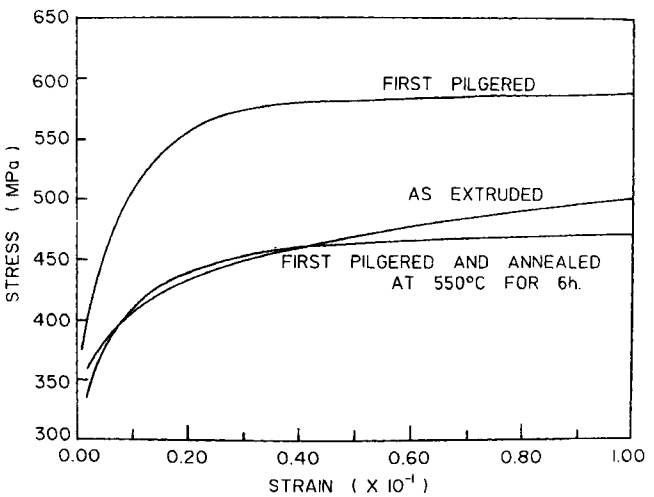

Fig. 11—True stress-strain plot for the as-extruded, the first pilgered, and the annealed (550 °C for 6 h) materials, demonstrating that the flow stresses of as-extruded and as-annealed materials at different levels of plastic strains are nearly the same.

low. Annealing at 550 °C for 6 hours caused nearly complete recrystallization of the α stringers without altering the original elongated $\alpha + \beta_I$ microstructure (Figure 10(b)). It could be seen from Table IV that the tensile strength and elongation values at 310 °C after annealing at 550 °C were similar to those of hot-extruded tubes. A comparison of the true stress-strain plot for the as-hot-extruded and the as-annealed materials, shown in Figure 11, demonstrates that the flow stresses at different levels of plastic strains of this material in these two conditions are nearly the same. Both these observations suggest that the cold work introduced during the first pilgering step is completely annihilated by the annealing treatment at 550 °C for 6 hours. In contrast to this, annealing at 600 °C even for 1 hour resulted not only in complete recrystallization of the α and β_I constituents but also in a marked change in the morphology of these two phases (Figure 10(c)). The grains of the α phase became nearly equiaxed and the β_I phase was noticed primarily at the boundaries and trijunctions of α grains. The significant coarsening of structure, which accompanied the morphological changes due to annealing, appears to be responsible for the decrease in the tensile strength of the alloy to a level below that of the hot-extruded material (Table IV). On the basis of the tensile properties and the morphology of the two-phase structure, it could be concluded that annealing at 550 °C for 6 hours would be appropriate

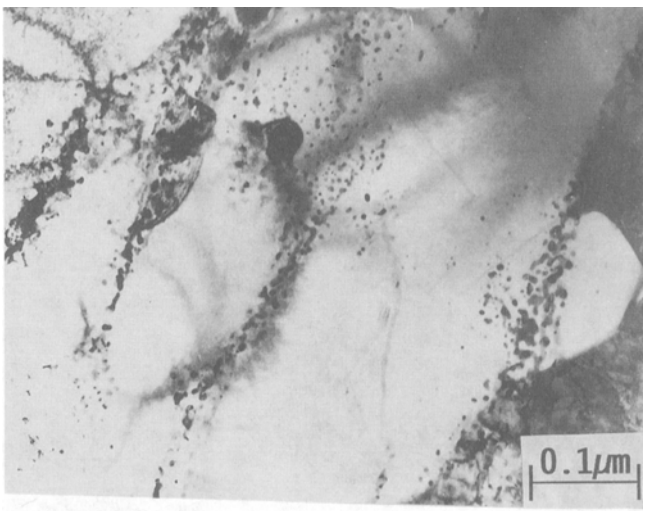

Fig. 12—Micrograph showing the fragmentation and spheroidization of the β_I phase after annealing at 550 °C for 3 h.

to achieve the desired results of the intermediate annealing treatment.

It was noticed that the volume fraction of the β_I phase was considerably reduced after the annealing treatment. The heavy cold working during the first pilgering step was responsible for the thinning of the β_I layers between neighboring α stringers. This effect, together with the enhanced diffusivity due to high dislocation density, could aid the partitioning of niobium atoms between the metastable $\beta(\beta_I)$ and α phases. Using the free energy composition plot computed for the Zr-Nb system,[12] one could see that the niobium content of the β_I phase would tend to increase to a level of about 20 pct. Further niobium enrichment, however, would be difficult in view of the large free energy hump existing between the β_I and β_{II} phases. Annealing at a temperature of 550 °C or higher could cause precipitation of the α phase within the β_I layers and dissolution of ω particles. These processes would essentially lead to the thinning of the β_I layers and disappearance of the ω phase, as observed. Due to the absence of the first pilgering and annealing stages in the conventional fabrication route, the enrichment of the β_I phase is not expected to occur, resulting in a higher volume fraction of the β_I phase just before the cold drawing operation. In this case, if the β_I phase is formed in some regions during the hot extrusion stage, it will remain in the structure even during subsequent processing stages.

The microstructure of annealed samples showed a distribution of fine β_I particles predominantly at the interfaces of the α stringers (Figure 12). Such fine precipitates were not observed either in the hot-extruded or in the first pilgered material. The fragmentation and spherodization of the β_I layers were motivated by the chemical free energy change associated with the niobium enrichment of the β_I phase and by interfacial energy reduction. The absence of β_I precipitates within the α stringers suggested that the niobium content of the α stringers produced during hot extrusion was close to the equilibrium solubility of niobium in the α phase at 550 °C. Similar modification of the morphology and composition of the β_I phase is unlikely to occur in the conventional route due to the absence of these two fabrication stages.

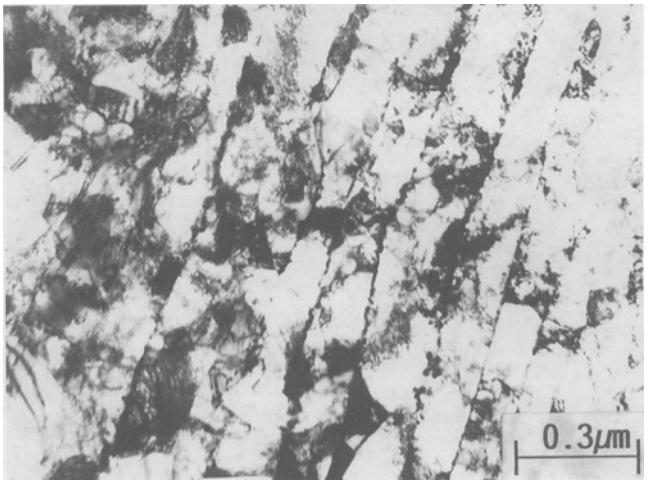

Fig. 13—Micrograph showing the presence of very thin layers of β_I phase between the α stringers in the longitudinal section after the second pilgering.

Table V. Basal Pole Texture Coefficient of Pressure Tubes

Fabrication Route	Axial	Radial	Circumferential
Modified	0.3 to 0.6	1.1 to 2.3	2.4 to 4.0
Conventional[1]	0.5 to 1.0	1.0 to 2.0	>1.0

VII. SECOND PILGERED AND AUTOCLAVED STRUCTURE

The second pilgering step which follows the intermediate annealing treatment introduces 20 to 25 pct cold work and imparts the final dimensions to the pressure tube. Figure 13 is a representative TEM micrograph corresponding to the longitudinal section of a pressure tube which has-seen the second pilgering step. It can be seen that the elongated morphology of the two phases generally remained unaltered. The dislocation arrangement at the interfaces of the two-phase structure and within the two phases, developed during the various stages of fabrication, plays an important role in the performance of the pressure tube in the reactor, particularly in controlling properties such as resistance to irradiation creep and growth.[26]

The dislocation density in the final microstructure of the pressure tube material was estimated by imaging dislocations from the same area at different specimen tilts in TEM so as to obtain a reliable average value. The average dislocation density was found to be in the range of 1 to 5 $\times$ 10^{14} lines/m^2, which is very close to the dislocation density 5 to 7 $\times$ 10^{14} lines/m^2 reported in the pressure tubes fabricated by the conventional route.[1]

The crystallographic texture developed during the fabrication of the pressure tube is very important with reference to irradiation creep, irradiation growth, hydride orientation, and mechanical properties.[1–7,27] It has been reported that the crystallographic texture developed during hot extrusion is essentially retained during the subsequent fabrication stages of these tubes through the modified route.[25] In the present work, the crystallographic texture was determined using the method described by Harris,[28] in which diffraction intensities from samples sectioned perpendicular to representatives of these three principal directions of the pressure tube are compared with those from a sample having a random texture. Since the direction of the basal plane normal is important for relating the texture to various material properties, texture coefficients for the basal poles were measured and the results are presented in Table V. The majority of the basal poles in the pressure tube are oriented in the circumferential direction and, to some extent, in the radial direction. A somewhat lower value of the basal pole texture coefficient in the circumferential direction was obtained as compared to that reported for the conventionally processed material.[1] This could be attributed to the lower extrusion ratio employed in the modified fabrication route and will result in a greater resistance to irradiation growth.[6]

The final autoclaving treatment at 400 °C for 72 hours is given for forming a strong and stable surface oxide film for a better in-reactor corrosion resistance. This treatment does not modify the microstructure developed during the previous fabrication steps, which is the same in both routes.

VIII. INTERFACE STRUCTURE

Various types of interfaces were encountered in this study. A detailed examination was carried out of the α/α interfaces, with due emphasis on the dislocation arrangement at these interfaces. The low-angle boundaries developed in the α phase due to recovery processes were also examined. High resolution electron microscopy was carried out at the α/β_I interfaces in order to identify the atomic registry at these interfaces.

The dynamically recrystallized $\alpha + \beta_I$ microstructure of the hot-extruded material showed that the β_I phase was almost exclusively present at the α boundaries. Such a structure could be classified as a dual-phase structure according to Hornbogen's definition of different types of two-phase microstructures.[29] The fact that the α/β_I interfaces replace some of the α/α interfaces suggests that the interfacial energy of the former was lower than that of the latter. The wetting of the α grain boundaries by β_I phase could be seen in Figure 6, where the β_I film tends to penetrate along α/α grain boundaries from the grain corners.

Two sets of parallel dislocations were frequently encountered at the α/β_I interfaces (Figure 14). The closely spaced set of dislocations (with an average spacing of about 5.0 nm) was visible under both $\{0002\}_\alpha$ and $\{10\bar{1}0\}_\alpha$ operating reflections, suggesting that these dislocations are of $\langle c + a \rangle$ type. The widely spaced dislocations, which are of $\langle a \rangle$ type, in conjunction with closely spaced dislocations generate an interfacial structure which closely resembles the α/β_I interfaces of Widmanstätten α plates.[8] Figure 15(b) shows a lattice resolution image of the α and adjoining β_I phase in a specimen of Zr-2.5 pct Nb alloy in which dynamic recrystallization has occurred during hot extrusion. It could be inferred from lattice resolution images such as this that the two lattices obeyed a Burgers orientation relationship[30]. The planar matching between $(0001)_\alpha$ and $(110)_{\beta I}$ was found to be near perfect (within 0.5 deg), suggesting the Burgers relationship rather than the Potter relationship.[31] Lattice registry and ledges could be seen at the α/β_I interfaces in this image (near arrow). The ledges seen in this view are three to five layers of basal planes. It appeared that the interfaces across which near-Burgers lattice correspondence was maintained provided a low energy

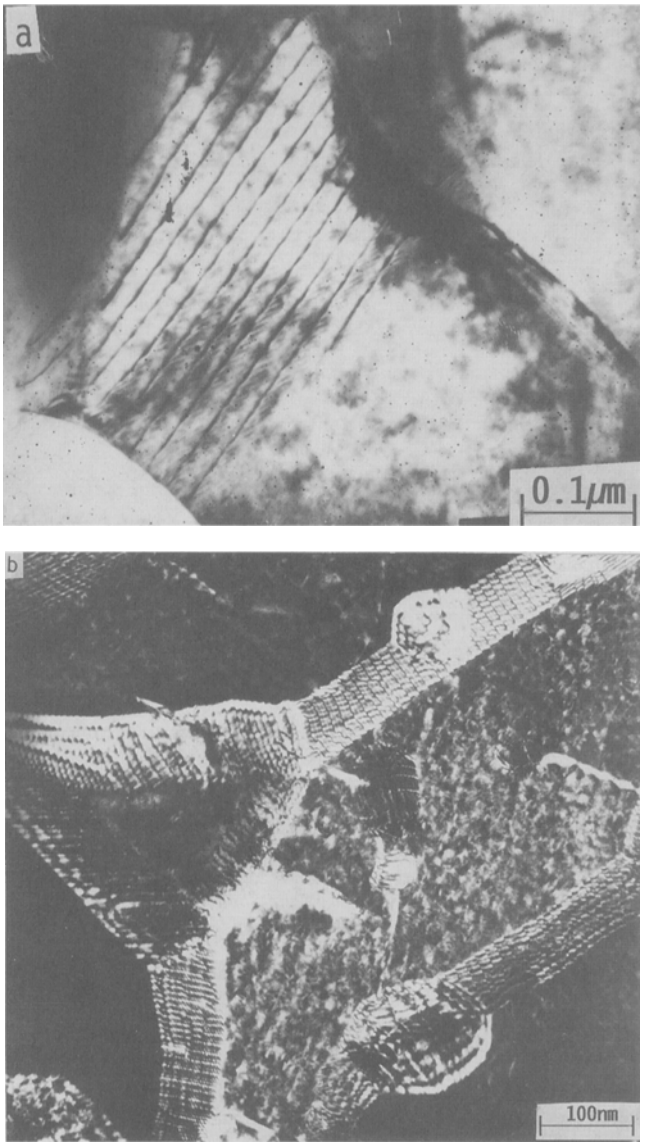

Fig. 14—(*a*) Arrays of the closely spaced $\langle c + a \rangle$ type of interfacial dislocations and widely spaced $\langle a \rangle$ dislocation at a β_I/α interface. (*b*) TEM micrograph showing a typical α/β_I interfacial dislocation network in a Widmanstättan structure consisting mainly of $\langle a \rangle$ and $\langle c + a \rangle$ type dislocations.

configuration. Because the volume fraction of β_I is larger, the fraction of α/β_I interfaces is higher in this modified route. Replacement of a random α/α boundary by such interfaces is expected to result in some energy savings. These interfaces would also be amenable to migration, allowing growth and decay of the adjacent phases.

The α/β_I interfaces formed in different phase reactions, such as Widmanstätten α precipitation from β_I,[14] precipitation of β_I from supersaturated α' martensite, and dynamic recrystallization of the α and β_I structure in Zr-Nb alloys, exhibit remarkable similarities. It has been shown[14] that the line vectors of interfacial $\langle c + a \rangle$ dislocations are often aligned along the invariant line strain (ILS) direction associated with the β_I/α transformation. This observation highlights the importance of the ILS condition in realizing the α to β_I transformation in either direction. In the context of the various diffusional processes mentioned earlier, the

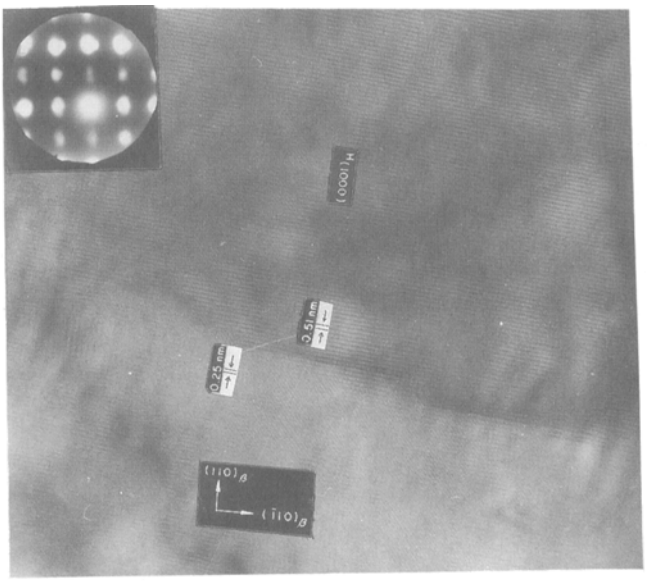

Fig. 15—High resolution electron micrograph showing perfect matching of α and β_I lattices at an α/β_I interface.

migration of α/β_I boundaries could be viewed in terms of the movement of $\langle c + a \rangle$ dislocations which are parallel to the ILS direction and lie on the common $(101)_{\beta I}//(10\bar{1}1)_\alpha$ plane. The lattice invariant shear in the β_I to α' martensitic transformation is also achieved by the same shear system.[32] The rotation of this type of α/β_I interfaces involves the introduction of a second set of $\langle a \rangle$ dislocations, the line vectors of which decide the axis of rotation.[3,14]

This type of special α/β_I interfaces, encountered very frequently in the hot-extruded (dynamically recrystallized) and annealed (statically recrystallized) material, not only provide a coherent low energy interface but also allow the growth of one phase at the expense of the other, accompanied by partitioning of the niobium atoms. Since the hot extrusion step in the conventional and modified route is essentially the same (the only difference being the variation in the extrusion ratio), the frequent occurrence of the Burgers relation between the adjacent α/β_I grains and the nature of the special α/β_I interface are similar in both cases.

IX. CONCLUSIONS

An improved process for fabrication of Zr-2.5 Nb tubes has been developed which will provide lower irradiation growth and increase production yields. Specific details of the microstructure are as follows.

1. The β-quenched structure in Zr-2.5 pct Nb tubes consists of acicular martensite in which three distinct types of morphologies exist. These are large primary martensite plates which are occasionally internally twinned, fine secondary martensite plates arranged in self-accommodating groups, and martensite laths stacked almost parallel within a packet. The microstructure of this is the same in both fabrication routes.
2. During hot extrusion, the α and β_I phases dynamically recrystallize; β_I phase layers are sandwiched between α stringers. The aspect ratio of both phases are considerably lower than conventional processing, which will produce lower irradiation growth. The volume fraction of the β_I

phase is higher and the niobium content is lower than those obtained in conventionally processed tube. The ω-phase precipitates within the β_l during cooling of the hot-extruded tubes following either processing route.

3. The first pilgering operation further elongates both α and β_l microstructures, and during the subsequent annealing treatment, static recrystallization of the two phases occurs. The optimum annealing treatment (550 °C for 6 hours) retains the elongated morphology of the two phases produced in the hot extrusion step. The tensile strength at 310 °C of the annealed product also remains at the same level as that attained after hot extrusion.

4. The special type of α/β_l interface frequently observed in both dynamically and statically recrystallized materials provides a low energy configuration in which the Burgers orientation relationship is obeyed between the α and β_l phases and the lattice registry is maintained across the interface. The nature of the α/β_l remains the same in either processing route.

5. The improved microstructure due to the additional processing steps provides a better control of dimensional tolerances, less variability in the finished product, and tighter control of mechanical properties.

ACKNOWLEDGMENTS

The authors wish to thank Messrs. K. Balaramamoorthy and P. Pande and other colleagues at the Nuclear Fuel Complex, Hyderabad, for supplying samples from different stages of pressure tube fabrication and for continuous exchange of information. The help received from Mr. J.B. Singh with the quantitative metallography is gratefully acknowledged. Thanks are due to Dr. S.J. Vijaykar, Messrs. V.V. Raman and Madangopal K., and Dr. P. Mukhopadhyay for many helpful discussions during several phases of this work.

REFERENCES

1. B.A. Cheadle, C.E. Coleman, and H. Licht: *Nucl. Technol.*, 1982, vol. 57, pp. 413–25.
2. R.G. Fleck, E.G. Price, and B.A. Cheadle: *Zirconium in the Nuclear Industry*, ASTM STP 824, D.G. Franklin and R.B. Adamson, eds., ASTM, Philadelphia, PA, 1984, pp. 88–105.
3. B.A. Cheadle: *Zirconium in the Nuclear Industry*, ASTM STP 633, A.L. Lowe, Jr. and G.W. Parry, eds., ASTM, Philadelphia, PA, 1977, pp. 457–85.
4. R.A. Holt: *J. Nucl. Mater.*, 1979, vol. 82, pp. 419–29.
5. R.G. Fleck: *Can. Metall. Q.*, 1979, vol. 18, p. 65.
6. E.F. Ibrahim and R.A. Holt: *J. Nucl. Mater.*, 1980, vol. 91, pp. 311–21.
7. R.A. Holt and E.F. Ibrahim: *Acta Metall.*, 1979, vol. 27, pp. 1319–28.
8. V. Perovic, G.C. Weatherly, and C.J. Simpson: *Acta Metall.*, 1983, vol. 31, pp. 1381–91.
9. V. Perovic, G.C. Weatherly, and R.G. Fleck: *Can. Metall. Q.*, 1985, vol. 24, pp. 253–57.
10. E. Tenchhoff: *Deformation Mechanism, Texture, and Anisotropy in Zirconium and Zircaloy*, ASTM STP-966, ASTM, Philadelphia, PA, 1980.
11. J.P. Abriata and J.C. Bolcich: *Bull. Alloy Phase Diagrams*, 1982, vol. 3, pp. 34–44.
12. Sarath Kumar Menon, S.K. Banerjee, and Rangachari Krishnan: *Metall. Trans. A*, 1978, vol. 9A, pp. 1213–20.
13. V. Perovic and G.C. Weatherly: *Acta Metall.*, 1989, vol. 37, pp. 813–21.
14. S. Banerjee, G.K. Dey, and S.J. Vijayakar: *Int. Proc. Indo-American Workshop on Interface*, Oxford and IBH Publishing Co., New Delhi, India, 1990.
15. C.P. Luo and G.C. Weatherly: *Metall. Trans. A*, 1988, vol. 19A, pp. 1153–62.
16. S. Banerjee and R. Krishnan: *Acta Metall.*, 1971, vol. 19, pp. 1317–26.
17. C.D. Williams and R.W. Gilbert: *J. Nucl. Mater.*, 1966, vol. 18, pp. 161–66.
18. D. Srivastava, K. Madangopal, S. Banerjee, and S. Ranganathan: *Acta Metall. Mater.*, 1993, vol. 41, pp. 1445–54.
19. J.K. Chakravartty, G.K. Dey, and S. Banerjee: *Materials Sci. and Tech.*, 1995, (In press).
20. S.L. Sass: ONR Technical Report '62 Contract No. N00014-67-A-0077–0012, 1971.
21. R.F. Hehemann: *Can. Metall. Q.*, 1972, vol. 11, pp. 201–12.
22. R. Strychor and J.C. Williams: *Solid-Solid Phase Transformations*, H.I. Aaranson, D. Laughlin, R.F. Sekerka, and C.M. Wayman, eds., TMS, Pittsburgh, PA, 1981, pp. 249–53.
23. L.A. Benderskey, W.J. Boettinger, R.P. Burton, F.I. Biancaniello, and C.B. Shoemaker: *Acta Metall. Mater.*, 1990, vol. 38, pp. 931–43.
24. B.A. Cheadle, C.E. Ells, and W. Evans: *J. Nucl. Mater.*, 1967, vol. 24, pp. 199–208.
25. A.J. Haq, A. Haq, and S. Banerjee: *Bull. Mater. Sci.*, 1992, vol. 15, pp. 289–96.
26. E.F. Ibrahim and B.A. Cheadle: *Can. Metall. Q.*, 1985, vol. 24, pp. 273–81.
27. E.F. Ibrahim: *J. Nucl. Mater.*, 1983, vol. 118, pp. 260–68.
28. G.B. Harris: *Phil. Mag.*, 1952, vol. 43, pp. 113–23.
29. E. Hornbogen, *Int. Mater. Rev.*, 1989, vol. 34, pp 277–296.
30. W.G. Burgers: *Physica*, 1930, vol. 1, pp. 561–86.
31. D.I. Potter: *J. Less-Common Met.*, 1973, vol. 31 p. 299.
32. H.M. Otte: *The Science Technology and Application of Titanium*, R.I. Jaffee and N.E. Promisel, eds., Pergamon, London, 1970, pp. 645–57.